JOURNAL OF SYNCHROTRON RADIATION
ISSN 1600-5775

Reducing the thermal deformation of InSb crystal by using double-bounce HHRMs in the TPS tender X-ray absorption spectroscopy beamline

Din-Goa Liu, Ming-Han Lee, Ying-Jui Lu, Jyh-Fu Lee and Chi-Liang Chen*

National Synchrotron Radiation Research Center, 101 Hsin-Ann Road, Hsinchu Science Park, Hsinchu 30076, Taiwan. *Correspondence e-mail: chen.cl@nsrrc.org.tw

Received 9 December 2020
Accepted 14 April 2021

Edited by D. Bhattacharyya, Bhabha Atomic Research Centre, India

Keywords: double-bounce HHRMs; tender XAS; thermal load; InSb crystal.

Supporting information: this article has supporting information at journals.iucr.org/s

The Taiwan Photon Source (TPS) with high brightness and energy tunability is suitable for applications in spectroscopy. The tender X-ray absorption beamline will be optimized for X-ray absorption spectroscopy measurements using a bending-magnet source in a unique photon energy range (1.7–10 keV) and two crystal pairs [InSb(111) and Si(111)] separated using back-to-back double-crystal monochromators (DCMs). InSb crystals are typically used in the lower photon energy range of 1.7–3.5 keV. However, the poor thermal conductivity of InSb crystals leads to severe deformation. This factor should be considered when the monochromator is installed on a tender X-ray beamline in a storage ring with a high power density. There are many approaches to reducing the thermal load on the first crystal of a DCM. Double-bounce high harmonics rejection mirrors in front of the DCM serve not only to reduce the high-order harmonics but also to absorb considerable quantities of heat. Two coating stripes on the silicon surfaces with a variable incident angle will be key to solving the thermal load on this beamline.

1. Introduction

Some of the world's advanced synchrotron radiation light source facilities are dedicated to building tender X-ray beamlines with unique energy ranges (Cowan *et al.*, 1989; Northrup, 2019; Flank *et al.*, 2006; Kavčič *et al.*, 2012; Hu *et al.*, 2010; Du *et al.*, 2015). A tender X-ray absorption spectroscopy beamline will be built under the Phase III beamlines construction project of Taiwan Photon Source (TPS), National Synchrotron Radiation Research Center (NSRRC), Taiwan. The TPS, a third-generation synchrotron facility, operates at 3 GeV with a ring circumference of 518.4 m. The radius of each bending magnet (BM) is designed to be 8.35 m, corresponding to a magnetic field of 1.198 T, so as to have a critical energy of 7.17 keV. The total power of the BM source at TPS running at a ring current of 500 mA (with a 20% safety margin) is 133.0 W, using a mask of 2.1 mrad × 0.27 mrad at 21 m, and 101.3 W, using a mask of 2.1 mrad × 0.17 mrad at 21 m. As the TPS storage ring has low emittance, this results in higher and more concentrated flux. Two double-crystal monochromators (DCMs) are used in the tender photon energy range (1.7–10 keV). A Si(111) crystal pair is used at photon energies above 2100 eV, while the lower energy range (down to 1700 eV) can be covered by InSb(111) crystals (Hussain *et al.*, 1982; Dann *et al.*, 1998; Karlin *et al.*, 1994). The two DCMs can be selected depending on the experimental requirements. A double-bounce higher harmonic rejection mirrors (HHRMs) system has a key role in this beamline design and will reduce the thermal load and cut off the high-order harmonics. High-order harmonics are particularly

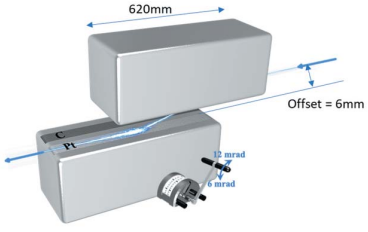

Table 1
Absorbed power on the beamline optics for different conditions of the source, with and without the Be window and HHRMs.

Source (h × v) (mrad)	Photon energy (keV)	Absorbed power (W)							DCM slope error (sagittal × tangential) (μrad)	Focal point beam size (h × v) (mm)	Flux (photon s^{-1})
		Integrated power (W)	Be window 100 μm	HHRM1	HHRM2	CM (7.5 mrad)	Second InSb(111) crystal	First Si(111) crystal			
2 × 0.25	1.7 (InSb)	121.9	–	–	–	–	–	–	–	–	3×10^{13}
2 × 0.25	1.7 (InSb)	121.9	–	–	–	64.1	57.8	–	360.6 × 194.7	37 × 17	4.9×10^{10}
2 × 0.25	2.1 (Si)	121.9	–	–	–	64.1	–	57.8	19.7 × 11.4	1.7 × 1.4	4.4×10^{10}
2 × 0.15	1.7 (InSb)	88.3	–	–	–	49.9	38.4	–	254.8 × 130.6	25 × 12	6.4×10^{10}
2 × 0.15	1.7 (InSb)	88.3	9.5	–	–	48.3	30.5	–	199.5 × 101.8	19 × 10	6.7×10^{10}
2 × 0.15	2.1 (Si)	88.3	9.5	–	–	48.3	–	30.5	10.7 × 6	0.7 × 0.5	4.6×10^{10}
2 × 0.15	1.7 (InSb)	88.3	9.5	76.1 @ 10.5 mrad (C)	0.7 @ 10.5 mrad (C)	0.5	1.5	–	9.2 × 4.6	0.85 × 0.7	6.6×10^{10}
2 × 0.15	3.0 (InSb)	88.3	9.5	74.3 @ 9 mrad (C)	0.9 @ 9 mrad (C)	0.8	2.8	–	15.9 × 8.7	0.9 × 1.1	1.5×10^{12}
2 × 0.15	2.1 (Si)	88.3	9.5	74.3 @ 9 mrad (C)	0.9 @ 9 mrad (C)	0.8	–	2.8	0.9 × 0.5	0.1 × 0.24	4.2×10^{10}
2 × 0.15	3.0 (Si)	88.3	9.5	66.3 @ 6 mrad (C)	1.5 @ 6 mrad (C)	2.3	–	8.7	2.7 × 1.5	0.2 × 0.3	4.0×10^{11}
2 × 0.15	4.0 (Si)	88.3	9.5	50.8 @ 8 mrad (Pt)	7.9 @ 8 mrad (Pt)	4.4	–	15.6	4.7 × 2.8	0.2 × 0.33	5.6×10^{11}

problematic for beamline designs below 10 keV. It is well known that the existence of high-order harmonics in the synchrotron radiation source would cause serious spectral distortion when the X-ray absorption spectra (XAS) are collected (Lamble, 1995; Sainctavit *et al.*, 1988). Therefore, it is the primary goal of the beamline to record a proper absorption spectrum without the high-order harmonics at the experimental end-station.

Most tender X-ray beamlines with similar energy range designs use the first collimator mirror (CM) to absorb most of the heat from the source. These beamline designs use only CM and toroidal focusing mirror (TFM) coatings to suppress high harmonic signals, but it may not be easy to obtain a clean light source with a high harmonic rejection ratio (Cowan *et al.*, 1989; Northrup, 2019; Flank *et al.*, 2006; Kavčič *et al.*, 2012; Hu *et al.*, 2010; Du *et al.*, 2015). Moreover, double-bounce HHRMs are located downstream behind the TFM in the existing hard X-ray beamlines (Hayama *et al.*, 2018; Thompson *et al.*, 2009; Follath *et al.*, 2016; Caliebe *et al.*, 2019). Recently, a refractive optics method was proposed and used to reject higher-order harmonics to 1×10^{-3} at the ID06 beamline of ESRF (Polikarpov *et al.*, 2014). Further, there are three existing beamlines with double-bounce mirrors upstream of the DCM. They are the TES beamline of NSLS-II, the LUCIA beamline of LURE-SOLEIL, and the Phoenix I beamline of Swiss Light Source (Northrup, 2019; Janousch *et al.*, 2004). This design would be necessary to operate in the tender X-ray energy range, using poor thermal conductivity monochromatic crystals under high power density, and could effectively result in a higher harmonic rejection ratio.

InSb(111) crystals are commonly used to monochromate the X-ray source at lower energy, although the crystal has a deficient resolution ($\Delta E/E \simeq 3 \times 10^{-4}$ at 2 keV), and poor thermal conductivity causes thermal deformation issues (Rowen *et al.*, 1986; Yates *et al.*, 2010; Krumrey, 1998). A pair of InSb crystals will be selected based on consideration of the preferred semiconductor material and energy-related systems for measuring extended X-ray absorption fine structure (EXAFS) at the Si *K*-edge. The BM source at TPS has a higher power density than Taiwan Light Source, resulting in thermal deformation that diverges the monochromatic light and results in poor focusing of the TFM, in addition to greatly reducing the photon flux, as shown in Table 1. Thus, thermal analysis is the main task in designing a tender photon energy range beamline. The tender X-ray absorption spectroscopy beamline optical layout at TPS is shown in Fig. 1.

In the initial design, white-beam slits are used to receive a 2 mrad (h) × 0.25 mrad (v) BM source to obtain higher photon flux. However, the estimated integrated power on the first InSb crystal (at 29.6 m from the source) would be up to 57.8 W, from calculations using the *XOP* package (Table 1) (Sanchez del Rio & Dejus, 2004). Such a high power is very unfavorable to the operation of InSb crystals.

There are many considerations in the optical design of a beamline to reduce the thermal effects and power density on the crystal:

(*a*) Choose one or several filters with good thermal conductivity and appropriate thickness in the front-end to filter the heat generated below 1.7 keV. For this purpose, a water-cooled 100 μm-thick Be window (23 m from the source) is chosen as a filter to reduce the heating from low photon energies.

(*b*) Using a white-beam *X*–*Y* slit to reduce vertical or horizontal acceptance will reduce the power density but will also result in loss of flux. We choose to close the vertical slit slightly to 0.15 mrad, which reduces the power density and also does not affect the photon flux too much after optical calculation.

(*c*) A CM (27.1 m) with an incident angle of 7.5 mrad and a C/Pt bilayer coating (a 12 nm C layer on top of a 30 nm Pt

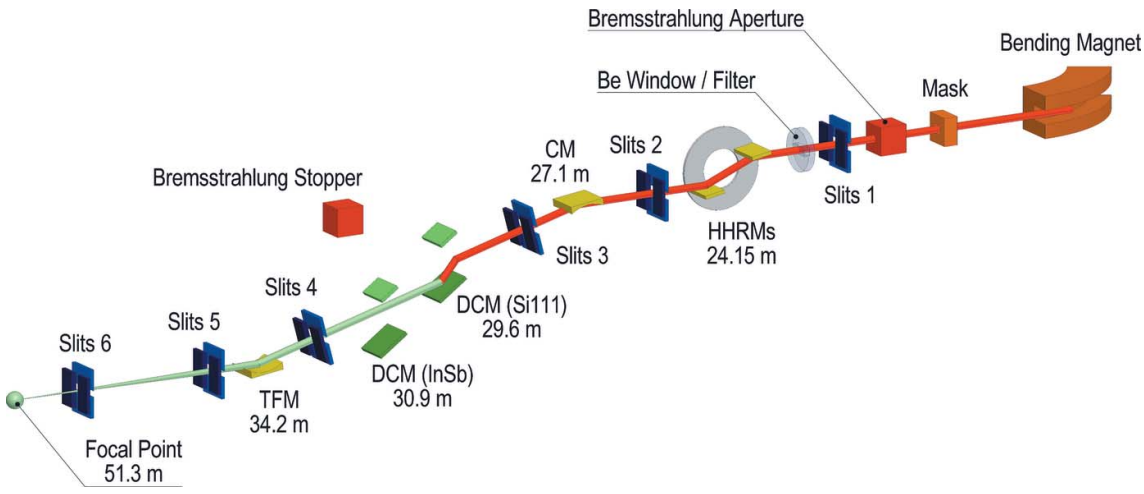

Figure 1
The envisioned TPS 32A beamline layout (side view) is illustrated showing the optical components. The entrance slit 1 uses an opening of 2 mrad (h) × 0.15 mrad (v). The first optical element of the beamline is a double-bounce HHRM (incident angle 6–12 mrad). The second mirror is a CM with C/Pt bilayer coating. After the CM, two crystal pairs DCMs, Si(111) and InSb(111), are used to efficiently cover the energy region 1.7–10 keV. The TFM focuses the beam to the sample position 51.3 m from the source in the end-station. The red arrow indicates white beam and the green arrow is the monochromatic beam.

layer) (Hu *et al.*, 2010) on the surface of the mirror could cover the energy range 1.7–10 keV and absorb heat above 10 keV upstream of the beamline. An increase in the incident angle of the CM would reduce the thermal load on the first crystal. However, that would reduce the available maximum photon energy range and would affect the original intention of this beamline specification.

(*d*) Double-bounce HHRMs could be used to solve the problems caused by thermal effects without reducing the available energy range, by increasing the incident angle of the CM or by sacrificing too much photon flux in the low-energy regions by adding filters. This is the main focus of this paper. Lessening the complexity of the optical design and maintaining a stable beam height with constant offset to the end-station are the key points in the design of the upcoming tender X-ray spectroscopy beamline (32A).

2. Finite-element analysis simulation

The optical design of the tender X-ray absorption spectroscopy beamline includes double-bounce HHRMs (23.9 and 24.4 m), a vertical CM, two DCMs and a TFM (34.2 m). In this design, double-bounce HHRMs are arranged in front of the CM to reduce the thermal load on the monochromator crystals and to suppress high-order harmonics contamination. The CM is for collimating the vertical divergence from the source. The two DCMs are followed by a 2:1 TFM, coated in the same way as the CM, which focuses the beam to the first sample position (focal point) 51.3 m from the source in the end-station (MacDowell *et al.*, 2004). The HHRM is typically set close to the focal point behind the monochromator and the mirror length can be shortened by the focused beam size in a hard X-ray beamline setup (Hayama *et al.*, 2018; Thompson *et al.*, 2009; Follath *et al.*, 2016). It is an easy installation without a cooling system for the monochromatic beam downstream. However, considering the poor thermal conductivity of the InSb(111) crystals used in this beamline, the double-bounce HHRMs system is employed as the first optical device from the source to dissipate the thermal load on subsequent optics. This is the approach taken at the NSLS-II TES and LURE-SOLEIL LUCIA beamlines (Caliebe *et al.*, 2019; Northrup, 2019). The double-bounce design (as opposed to single-bounce) can maintain the downstream beam's traveling direction parallel to the upstream beam, and the offset between the incident beam and the exit beam will remain constant regardless of the incident angle (in the range 6–12 mrad in this case). Therefore, as the user modulates the corresponding incident angle according to the required cut-off energy, all the downstream optical components can remain in place. Fig. 2(*a*) shows a conceptual drawing of double-bounce mirrors, which are mounted face-to-face on a rigid mechanism, like a well parallel channel-cut crystal system, with an overlap of 120 mm in length. Limited by the available space for the mirror system upstream of the beamline, the gap between the two HHRMs is set to 3 mm. As shown in Fig. 2(*b*), the incident angle of the HHRMs can be changed from 12 mrad to 6 mrad according to the required energy range by rotating the two mirrors simultaneously about a common axis in the center. The angle of the mirror system can be controlled using a stepper motor with an encoder that acts on the center of the mirror's support frame. This is mechanically much simpler than two independently moving mirrors, like at, for instance, the NSLS-II TES. The length of each HHRM is set to 620 mm to ensure that the light footprint (599.96 mm) at a low angle of 6 mrad can be completely received. The vertical acceptance angle of each mirror is 0.15 mrad. Hence, the double-bounce HHRMs system can keep the incident and the outgoing beams parallel with a constant offset of 6 mm.

To generate the required different energy cut-offs in the tender photon energy range, HHRMs require two different

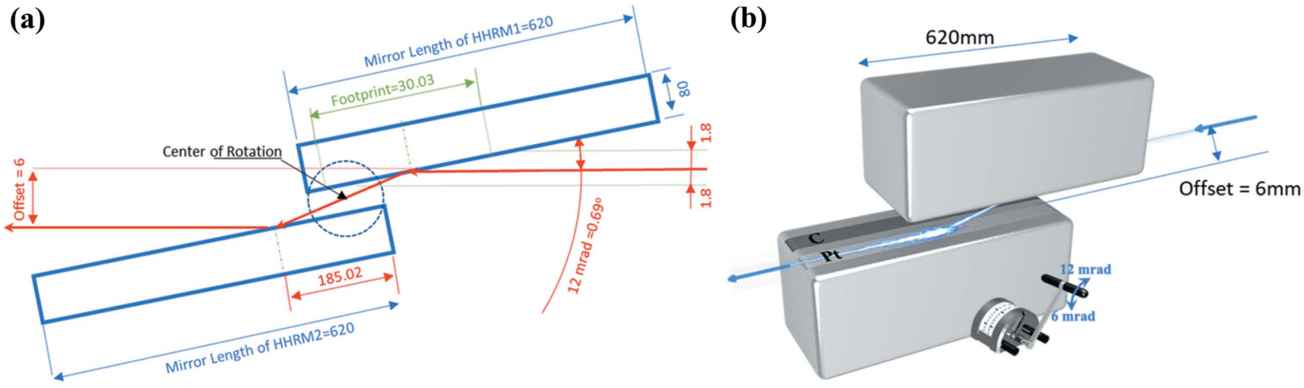

Figure 2
(*a*) Conceptual drawing of the double-bounce HHRMs at an incident angle of 12 mrad = 0.69°. (*b*) The C and Pt coating stripes on the HHRMs with a changeable incident angle from 12 mrad to 6 mrad.

coatings and a tunable angle of incidence. In addition to the bilayer coating of the CM and TFM to reduce the high-order harmonic ratio of the light, two independent parallel stripes, 30 nm of carbon (C) and platinum (Pt), have been chosen. Figs. 3(*a*) and 3(*b*) show calculations of the reflectivity of the C and Pt coatings, respectively, at different angles for the required cut-off energy. The photon energy required during each experiment determines the different coating stripes and incident angles for removing excess heat above the cut-off energy in use. As for working in the energy range 1.7–3 keV, since the Pt *M*-edge absorption edges would appear in the region from 2.1 to 3.3 keV, the carbon coating would be an option to cover this range with less intensity loss. For example, while running in the lower photon energy range (1.7–4 keV) from the Si (1839 eV) to Cl (2832 eV) *K*-edge for EXAFS measurements, the incident angle could be from 10.5 to 7.5 mrad using the C coating stripe [Fig. 3(*a*)]. Above 4 keV and up to 10 keV (the maximum photon energy of the beamline), the system can be horizontally shifted to use the Pt coating stripe and the incident angle can also be adjusted easily according to the measurement requirements, as shown in Fig. 3(*b*). The high-order harmonic ratio can be reduced to less than 1×10^{-4} to obtain a cleaner light source as the reflection characteristics of the coating layer of CM and TFM are at an incident angle of 7.5 mrad and combined with the variable incident angle double-bounce HHRMs (Table 2). Owing to the incident angle being quite small and hence a relatively large spot area is generated on the mirror surface that has the function of dispersing heat, the thermal deformation of the mirror surface is less. Simultaneously, most of the high-energy photons are removed by the first HHRM. This could ensure that the downstream optical elements (CM and the first crystal of the DCM) will not be deformed or even deteriorated by the excessive thermal load, which would affect performance, especially when using crystals with poor thermal conductivity in the DCM. According to the experimental conditions, the cut-off energy can be adjusted to the lowest acceptable value that is slightly higher than the upper limit of the energy scanning range. Moreover, relative to a single reflection, double reflections provide a much better removal efficiency.

As stated above, double-bounce HHRMs are used to remove thermal loads that are above the cut-off energy to be used. It is also necessary to remove heat from the energy range below 1.7 keV. The filter or attenuator mainly absorbs low photon energy (less than 1.7 keV) by using low-*Z* elements (carbon, diamond or Be foil). The demand for filters is quite important in beamline design for the tender energy range.

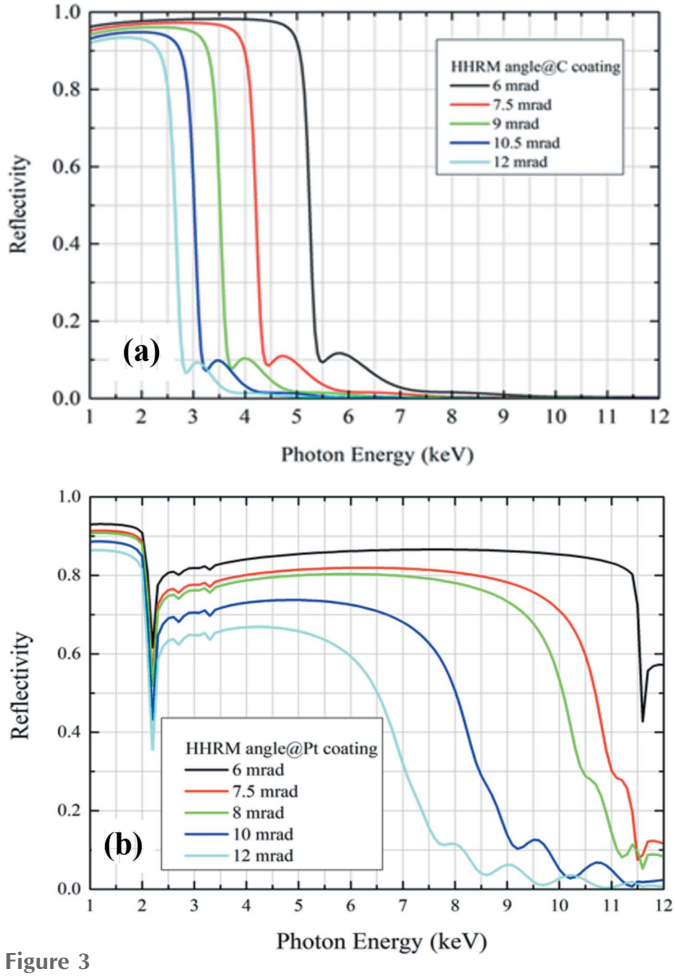

Figure 3
Reflectivity of the (*a*) Pt coating and (*b*) C coating at different incident angles as a function of energy from 1 to 12 keV.

Table 2
Ratio of the third harmonic contamination through the reflectivity of the four mirrors (HHRMs, CM and TFM) at the lowest energy in a specified range for various conditions of the HHRMs.

Energy range (keV)	HHRM1	HHRM2	CM and TFM	Ratio of third-order contamination
1.7–3.0	C (30 nm) on Si at 10.5 mrad	C (30 nm) on Si at 10.5 mrad		1.02×10^{-4} @ 1.7 keV
2.1–3.5	C (30 nm) on Si at 9 mrad	C (30 nm) on Si at 9 mrad		3.06×10^{-5} @ 2.1 keV
3.0–5.0	C (30 nm) on Si at 6 mrad	C (30 nm) on Si at 6 mrad	C(12.0 nm) / Pt(30 nm) / Si at 7.5 mrad	6.06×10^{-5} @ 3.0 keV
4.0–9.0	Pt (30 nm) on Si at 8 mrad	Pt (30 nm) on Si at 8 mrad		5.29×10^{-5} @ 4.0 keV
8.0–10.0	Pt (30 nm) on Si at 7.5 mrad	Pt (30 nm) on Si at 7.5 mrad		2.67×10^{-10} @ 8.0 keV

However, filters have the disadvantage of reducing the photon flux in the energy range 1.7–2 keV. Moreover, the choice of filter thickness is also crucial in the X-ray transmission calculation (Romanato *et al.*, 2001). In the simulation calculation, the ring current is set at 600 mA (20% higher than 500 mA of TPS) and the entrance white-beam slits use an opening of 2 mrad (h) × 0.15 mrad (v) so that the power would be 88.3 W in the extreme case. A 100 µm-thick Be window at 23 m can absorb 9.5 W power with a footprint of 46 mm (h) × 3.45 mm (v) (Table 1). Considering the vacuum safety of the beamline, it is more suitable to set up a water-cooled 100 µm-thick Be 52 mm (h) × 6.5 mm (v) window (with vacuum isolation function) upstream of the double-bounce HHRMs. Therefore, even if there is outgassing from the HHRMs at the beginning of beamline commissioning, it should not affect the vacuum condition of the storage ring. The results of an integrated power analysis obtained using the *SolidWorks Simulation* software package (https://www.solidworks.com/product/solidworks-simulation) are displayed in Fig. 4. The results show that the maximum temperature is 313 K and the thermal stress distribution is 46 MPa at the center of the Be window, which is much lower than the safety margin of 240 MPa. Thermal analysis of the heat absorbed by the HHRMs at an incident angle of 10.5 mrad corresponding to 1.7 keV and with the CM at an incident angle of 7.5 mrad are shown in Table S1 and Figs. S1 and S2 of the supporting information.

From thermal analytic calculations using the *SolidWorks Simulation* software package, a comparison of different conditions can be obtained with and without the upstream double-bounce HHRMs to assess the thermal load and slope error of the first monochromator crystal (InSb and Si), as shown in Table 1. In the extreme case (without HHRMs) while running at 1.7 keV with a vertical white-beam slit opening of 0.15 mrad, the first InSb crystal is exposed to the white beam with a power density of 0.14 W mm^{-2} [the footprint on the first crystal is 4.16 mm (v) × 61.8 mm (h)] and a thermal load beyond 38 W. The InSb crystal would then deform with a large slope error of about 130.6 µrad (v) × 254.8 µrad (h). This estimation is consistent with the calculation and beamline commissioning results in the literature (Yates *et al.*, 2010). Cooling of the optical components of the CM that has an absorbed power of 49.9 W due to exposure to the white beam has been considered (Table 1). Such an extreme thermal condition due to the absorbed power is acceptable for Si(111) crystals with good thermal conductivity. However, such a design is not favorable for the InSb crystals since they cannot withstand such a high thermal power. Hence, when using an InSb crystal, it is a good idea to set up the optical element of the double-bounce HHRMs with a water-cooling system in front of the CM. In comparison with Table 1, the first mirror with C stripes at angle 10.5 mrad can absorb a power of 76.1 W (Fig. S1), which is 86% of the power under the same photon energy condition at 1.7 keV. Finite-element analysis (FEA) results of the first HHRM show that the slope error is 2.2 µrad (v) × 3.4 µrad (h) under the present design. The second HHRM and CM can absorb a power of 0.7 W and 0.5 W, respectively, and the resulting slope errors are less than 0.1 µrad (Figs. S2 and S3). Therefore, the double-bounce HHRMs not only greatly reduce the thermal load on the first InSb crystal of the monochromator, which can be decreased to 1.5 W with an acceptable slope error down to 4.6 µrad (v) ×

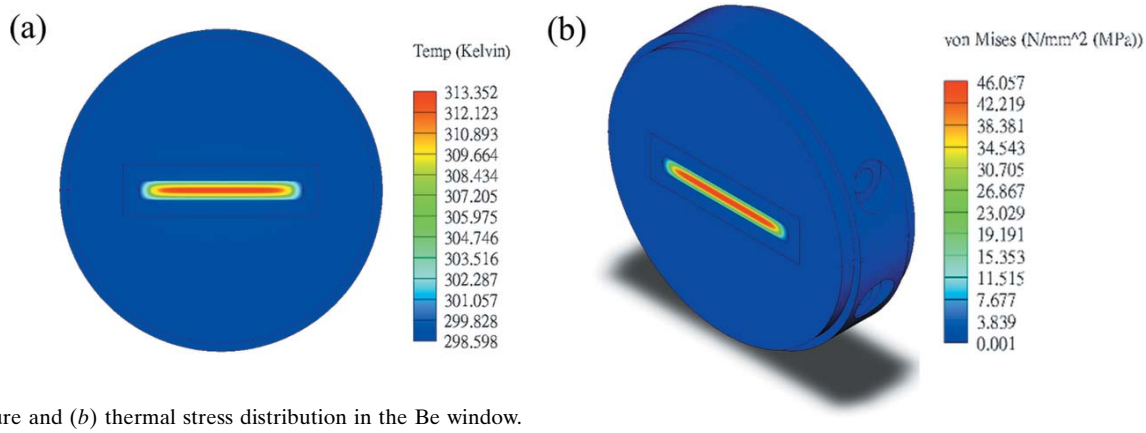

Figure 4
(*a*) Temperature and (*b*) thermal stress distribution in the Be window.

9.2 µrad (h), but also reduce the thermal load of the downstream CM with bilayer coating, meanwhile improving the collimation of the beam source to provide a better energy resolution. This high-quality condition is more suitable for photon energies of 2.1, 3 and 4 keV using a Si(111) crystal monochromator with much smaller slope error, as shown in Table 1.

Fig. 5(*a*) shows the case in which the CM, as the first optical mirror, is exposed to the white beam under the thermal load for the extreme case. The InSb(111) crystal size is 40 mm (L) × 75 mm (W). The thickness of the crystal is set at 2 mm, which refers to the actual measurement and calculation results by Hu *et al.* (Yates *et al.*, 2010; Hu *et al.*, 2010). The maximum Bragg angle is around 77.1° with a footprint of 4.16 mm (L) × 61.8 mm (W), in which the first crystal should absorb a power of 30.5 W (Table 1) in the extreme case of highest power density. The flow rate of 293 K cooling water was 2 L min^{-1}. The heat convection film coefficient was calculated to be 6390 W m^{-2} K for the FEA boundary conditions. The thermal contact conductance between oxygen-free high-conductivity copper (OFHC) block and InSb(111) crystal was set to 5000 W m^{-2} K (Marion *et al.*, 2006). The maximum tempera-

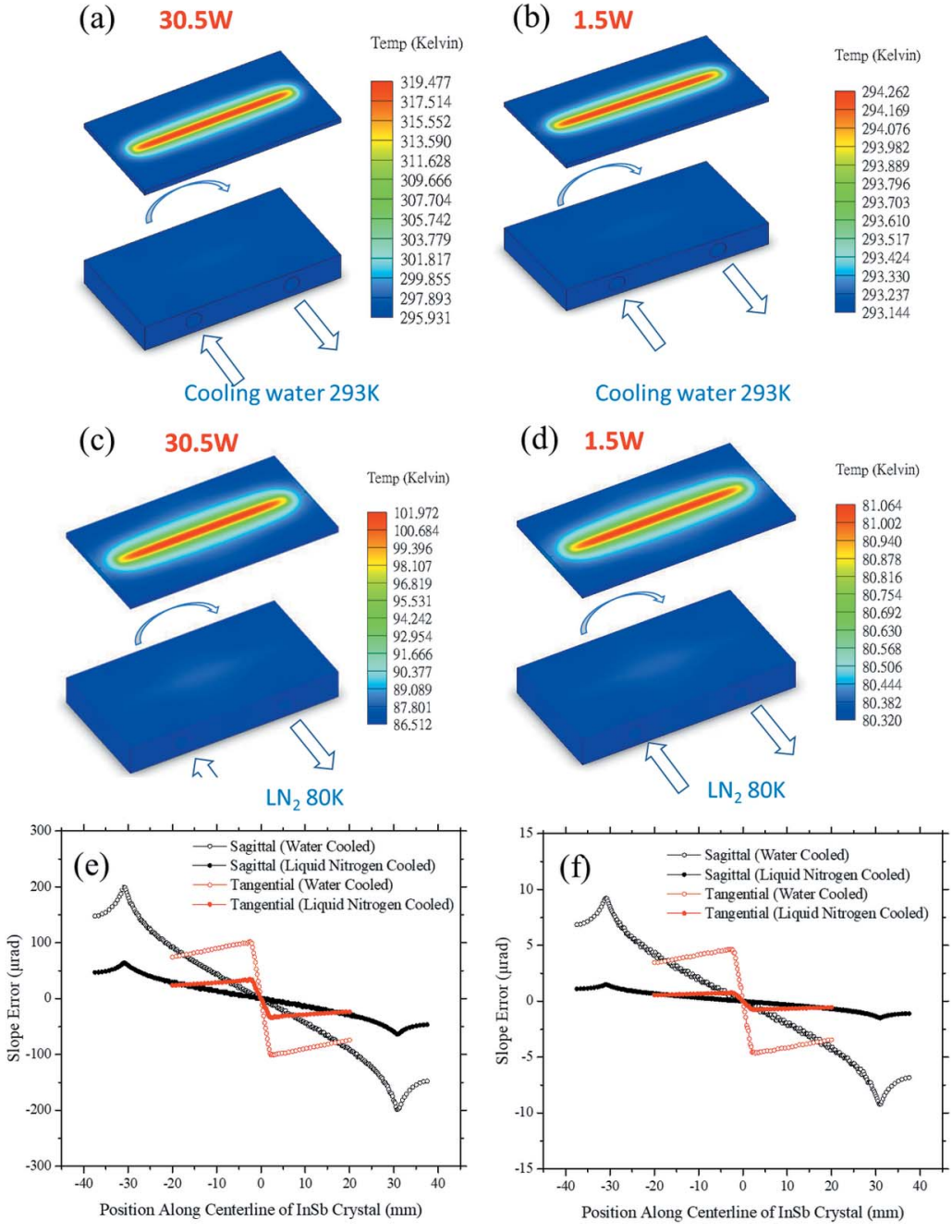

Figure 5
The FEA simulations results on the first InSb crystal which absorbed 30.5 W (without HHRMs) and 1.5 W (with HHRMs) at a photon energy of 1.7 keV. Temperature distribution with the water bottom cooling (*a*) without HHRMs and (*b*) with HHRMs. The temperature distribution with the LN_2 bottom cooling (*c*) without HHRMs and (*d*) with HHRMs. Slope error under the different cooling coolant (*e*) without HHRMs and (*f*) with HHRMs.

ture on the center of the crystal would be about 319 K and it is difficult to relieve the thermal load as shown by the blue color (lower temperature) surrounding the footprint in Fig. 5(*a*). This would cause thermal deformation. When the double-bounce HHRMs are set in front of the CM, the thermal load is largely absorbed by the first HHRM. The first InSb crystal of the downstream DCM only needs to absorb a power of 1.5 W, which reduces the maximum temperature to 294 K, as shown in Fig. 5(*b*). Setting different temperatures for the cooling water, the temperature difference caused by the same power on the InSb(111) crystal is almost unchanged, as the temperature of the cooling water is proportional to the slope error of the crystal (Yates *et al.*, 2010; Zhang *et al.*, 2013). Using the same conditions except for the cooling temperature, the simulation results with liquid nitrogen (LN_2) cooling (80 K) are displayed in Figs. 5(*c*) and 5(*d*). It can be observed that the temperature difference between the peak (red) and substrate (blue) value is decreased. Moreover, the comparisons of the slope error for water cooling (293 K) and LN_2 cooling (80 K) in the tangential and sagittal directions are shown in Figs. 5(*e*) and 5(*f*). Without the upstream HHRMs participating in heat absorption, the maximum slope error of the InSb crystal caused by the LN_2 cooling is 34.4 µrad (tangential). Under water-cooling conditions (293 K), the maximum slope error of the InSb crystal is only 4.6 µrad (tangential) because the upstream HHRMs eliminate most of the heat. This result implies that using double-bounce HHRMs to absorb heat is better than LN_2 cooling in this design. Therefore, using LN_2 to cool the crystal base will not significantly reduce the temperature gradient of the InSb crystal while the upstream HHRMs have absorbed most of the heat. Although LN_2 cooling can indeed further reduce slope errors, considering economic benefits and maintenance costs, LN_2 cooling is not considered as an option for this design. On the other hand, in comparison with the InSb(111) crystal, the Si(111) crystal reveals a better performance even with more than ten times heat power. The Si(111) crystal would absorb 57.8 W power using the vertical 0.25 mrad source without placing HHRMs in front of the DCM and displays a maximum temperature of 308.9 K at the center of the crystal. Even when the power level is lower than 30.5 W, the thermal deformation of indium antimonide is quite large because of its low thermal conductivity and large linear thermal expansion coefficient (Yates *et al.*, 2010). Accordingly, insertion of the double-bounce HHRMs in front of the CM and DCM is an effective way to decrease the thermal load on the crystal, and hence the overall beamline performance will reach an acceptable level. In the future, this design will be implemented at the tender X-ray absorption spectroscopy beamline in the TPS. Therefore, these necessary tasks and precautions must be carefully implemented, including mechanical structure design, operation mode, cooling mechanism, radiation assessment, accuracy and stability. The results of the beamline commissioning will be published in the near future. Although this beamline is under design for X-ray absorption spectroscopy, users will also require the hard X-ray photoelectron spectroscopy (HAXPES) technique to study specific chemical and electronic environments under the Fermi level (occupied states), which is also under planning. Various furnaces, cryostats and *in situ* cells for different sample environments will be available on request. All efforts are to provide diversified and user-friendly experimental conditions and environments to maximize scientific output.

3. Conclusion

The presented TPS 32A beamline mirrors concept is shown to minimize the thermal distortion of InSb(111) crystals. A double-bounce HHRMs system with variable setting grazing angle is crucial. This conceptual design provides a clean light source with very small high-order harmonic ratios down to 1×10^{-4}, reduces around 85% of thermal load on the downstream optical components, and yields a parallel exit beam to the incident beam with a constant offset independent of angle. A Be window is installed in front of the HHRMs to protect the ultra-high-vacuum environment of the front-end and to absorb the heat of low photon energies. Therefore, the proposal of a double-bounce HHRM in front of the DCM would provide an optical design concept for a wide range of spectroscopic measurement requirements, particularly at synchrotron facilities with a high-current storage ring.

Acknowledgements

The authors are grateful to Professor Krishna Kumar for proof-reading the manuscript and English corrections.

Funding information

This work was in part supported by the Ministry of Science and Technology (MoST) and National Synchrotron Radiation Research Center (NSRRC), Taiwan.

References

Caliebe, W. A., Murzin, V., Kalinko, A. & Görlitz, M. (2019). *AIP Conf. Proc.* **2054**, 060031.
Cowan, P., Brennan, S., Jach, T., Lindle, D. & Karlin, B. (1989). *Rev. Sci. Instrum.* **60**, 1603–1607.
Dann, T.-E., Chung, S.-C., Huang, L.-J., Juang, J.-M., Chen, C.-I. & Tsang, K.-L. (1998). *J. Synchrotron Rad.* **5**, 664–666.
Du, Y., Zhu, Y., Xi, S., Yang, P., Moser, H. O., Breese, M. B. H. & Borgna, A. (2015). *J. Synchrotron Rad.* **22**, 839–843.
Flank, A.-M., Cauchon, G., Lagarde, P., Bac, S., Janousch, M., Wetter, R., Dubuisson, J.-M., Idir, M., Langlois, F., Moreno, T. & Vantelon, D. (2006). *Nucl. Instrum. Methods Phys. Res. B*, **246**, 269–274.
Follath, R., Flechsig, U., Milne, C., Szlachetko, J., Ingold, G., Patterson, B., Patthey, L. & Abela, R. (2016). *AIP Conf. Proc.* **1741**, 020009.
Hayama, S., Duller, G., Sutter, J. P., Amboage, M., Boada, R., Freeman, A., Keenan, L., Nutter, B., Cahill, L., Leicester, P., Kemp, B., Rubies, N. & Diaz-Moreno, S. (2018). *J. Synchrotron Rad.* **25**, 1556–1564.
Hu, Y., Coulthard, I., Chevrier, D., Wright, G., Igarashi, R., Sitnikov, A., Yates, B., Hallin, E., Sham, T., Reininger, R., Garrett, R., Gentle, I., Nugent, K. & Wilkins, S. (2010). *AIP Conf. Proc.* **1234**, 343–346.
Hussain, Z., Umbach, E., Shirley, D., Stöhr, J. & Feldhaus, J. (1982). *Nucl. Instrum. Methods Phys. Res.* **195**, 115–131.

Janousch, M., Flank, A. M., Lagarde, P., Cauchon, G., Bac, S., Dubuisson, J., Schmidt, T., Wetter, R., Grolimund, G. & Scheidegger, A. (2004). *AIP Conf. Proc.* **705**, 312–315.
Karlin, B., Woicik, J. & Cowan, P. (1994). *Nucl. Instrum. Methods Phys. Res. A*, **347**, 360–363.
Kavčič, M., Budnar, M., Mühleisen, A., Gasser, F., Žitnik, M., Bučar, K. & Bohinc, R. (2012). *Rev. Sci. Instrum.* **83**, 033113.
Krumrey, M. (1998). *J. Synchrotron Rad.* **5**, 6–9.
Lamble, G. (1995). *Rev. Sci. Instrum.* **66**, 1422–1424.
MacDowell, A. A., Celestre, R. S., Howells, M., McKinney, W., Krupnick, J., Cambie, D., Domning, E. E., Duarte, R. M., Kelez, N., Plate, D. W., Cork, C. W., Earnest, T. N., Dickert, J., Meigs, G., Ralston, C., Holton, J. M., Alber, T., Berger, J. M., Agard, D. A. & Padmore, H. A. (2004). *J. Synchrotron Rad.* **11**, 447–455.
Marion, P., Zhang, L., Goirand, L., Rossat, M. & Martel, K. (2006). *Proceedings of the International Workshop on Mechanical Engineering Design of Synchrotron Radiation Equipment and Instrumentation 2006 (MEDSI2006)*, 24–26 May 2006, Himeji, Hyogo, Japan.
Northrup, P. (2019). *J. Synchrotron Rad.* **26**, 2064–2074.
Polikarpov, M., Snigireva, I. & Snigirev, A. (2014). *J. Synchrotron Rad.* **21**, 484–487.
Romanato, F., Di Fabrizio, E., Vaccari, L., Altissimo, M., Cojoc, D., Businaro, L. & Cabrini, S. (2001). *Microelectron. Eng.* **57–58**, 101–107.
Rowen, M., Waldhauer, A. & Pianetta, P. (1986). *Nucl. Instrum. Methods Phys. Res. A*, **246**, 440–443.
Sainctavit, P., Petiau, J., Manceau, A., Rivallant, R., Belakhovsky, M. & Renaud, G. (1988). *Nucl. Instrum. Methods Phys. Res. A*, **273**, 423–428.
Sanchez del Rio, M. & Dejus, R. J. (2004). *Proc. SPIE*, **5536**, 171–174.
Thompson, S., Parker, J., Potter, J., Hill, T., Birt, A., Cobb, T., Yuan, F. & Tang, C. (2009). *Rev. Sci. Instrum.* **80**, 075107.
Yates, B., Hu, Y. & Nagarkal, V. (2010). *Proc. SPIE*, **7802**, 78020U.
Zhang, L., Sánchez del Río, M., Monaco, G., Detlefs, C., Roth, T., Chumakov, A. I. & Glatzel, P. (2013). *J. Synchrotron Rad.* **20**, 567–580.